Reports in Mechanical Engineering
Vol. 4, No. 1, 2023, pp. 290-309
ISSN: 2683-5894, DOI: https://doi.org/10.31181/rme040129112023h

Some remarks on the two-dimensional contact of dissimilar elastic solids under non-slipping boundary conditions

Markus Heß [1]
[1] Department of System Dynamics and Friction Physics, Technische Universität Berlin, Germany,
e-mail: markus.hess@tu-berlin.de

Article Info

Article history:

Received October 23, 2023
Revised November 27, 2023
Accepted November 29, 2023

Keywords:

Contact mechanics,
Non-slipping contact,
Interface mismatch eigenstrain,
Similarity approach,
Partial slip,
Singular integral equations,
Dissimilar elastic materials.

ABSTRACT

Spence's self-similarity approach is often preferred to an incremental method for solving plane, non-slipping normal contacts of dissimilar elastic solids under progressive loading. The number of plane contact problems solved in this way so far is nevertheless very limited, since explicit expressions especially for the pressure distribution and the tangential tractions within the contact area require the solution of complicated singular integral equations. In contrast, the application of the incremental method leads to much simpler integral equations, which are derived here and applied to solve some new non-slipping contact problems including the one characterized by an initial power-law gap profile function. The incremental method is also capable to determine the so-called *interface mismatch eigenstrain*. In Spence's method, however, the determination of its magnitude represents a mandatory step within the solution procedure. By means of a comprehensive comparison of both methods this work provides new insights into the solution of non-slipping plane normal contact problems including explicit analytical solutions for the interface mismatch eigenstrain.

Corresponding Author:

Markus Heß,
Department of System Dynamics and Friction Physics, Technische Universität Berlin, Germany.
Email: markus.hess@tu-berlin.de

1. Introduction

When solving contact problems analytically, friction is often neglected, or bodies made of elastically similar materials are assumed. These two idealizing assumptions lead to Cauchy integral equations of the first kind, the solution of which is straightforward (Johnson, 1985). However, the solution is much more complicated if friction and/or elastic mismatch are taken into account, since this introduces coupling between normal and tangential effects. In practically all contact mechanics applications from the micro- to the macroscale tangential or frictional forces are present. As an example, take (wear) particles within the interface layer between two bodies that move relative to each other. When the wear particles come into contact with the surfaces of the two bodies, different contact states can arise, from partial slip to gross sliding or rolling (Li, 2020; de Payrebrune, 2022). Adhesion can also play a role and the corresponding tangential traction due to elastic mismatch would influence the adhesive behavior of particles. This is particularly important for applications on smaller scales such as cell adhesion, biological attachment devices (Chen & Gao, 2007) or designing of micro-electro-mechanical systems (MEMS) involving isotropic elastic solids and piezoelectric materials (Luo et al., 2022).

It is well known that even under pure external normal loading tangential tractions are generated within the contact area of two elastically dissimilar bodies. If a finite coefficient of friction is assumed, frictional slip in an edge region is inevitable. Such normal contact problems, involving a contact area composed of an inner stick and an outer slip area, can usually only be solved numerically. Spence (1973) gave a numerical solution

for the flat-ended punch contact with finite friction as well as an analytical solution neglecting the influence of the tangential tractions on the normal displacement and thus the pressure distribution (Goodman approximation). Spence has also proven that during progressive loading the ratio between the stick area and the contact area remains constant. Furthermore, this ratio is for all power-law indenters equal to the ratio obtained from the flat-ended punch problem. Nowell et al. (1988) solved the corresponding problem between dissimilar elastic cylinders. They also first provided an analytical solution applying the Goodman approximation and then a numerical solution based on Gauss Chebyshev quadrature. Zhupanska & Ulitko (2005) solved the same problem in a completely different mathematically complex way. They started from the general Papkovich-Neuber solutions, introduced very specific bipolar coordinates and apply the Wiener-Hopf technique to find solutions in the form of infinite series. Like Nowell et al., Zhupanska & Utlitko used Spence's self-similarity approach in order to specify the shape of the relative tangential strains within the stick regions.

The same approach is commonly used to develop analytical solutions for the simpler but still very complex limiting case of non-slipping normal contact where it is assumed that the coefficient of friction is sufficiently high to prevent any slip across the entire contact area. Adapted from the work of Spence (1968), Figure 1 shows an example of such a normal contact for the special case of one rigid and one elastic body. Material particles from the surface of the half plane exhibit different tangential displacements before they come into contact with the indenter during progressive loading. These tangential displacements remain unchanged in the course of further indentation and the associated growth of the contact area. This is illustrated in Figure 1 by the motion paths of surface particles. The dashed line indicates the location of the points that delimit the actual contact widths.

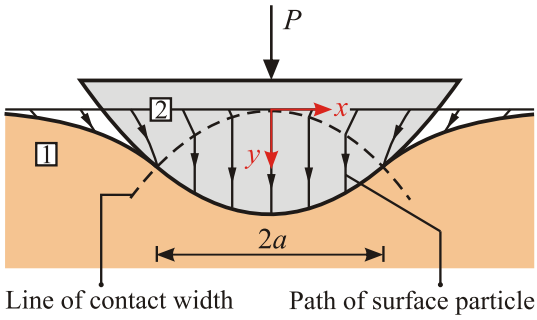

Figure 1. Indentation of a non-conformal rigid punch in the elastic half-plane under no-slip condition with indicated trajectories of surface particles during progressive loading

Several publications are dedicated to solving the axisymmetric non-slipping normal contact, often with additional consideration of molecular adhesion (Zhupanska, 2009; Borodich et al., 2014). Popov et al. (2019) provide a very simple and compact solution based on the method of dimensionality reduction (Popov & Heß, 2015; Heß, 2011). Popov (1973) and later Guo et al. (2011) accounted for the influence of an elastic half-space with a power-law grading. However, the pioneering works originate from Mossakovskii (1963) and Spence (1968). Plane normal contacts under full stick condition, on the other hand, have been treated less frequently and, apart from a few exceptions, there is a lack of explicit solutions. To the best of the author's knowledge, even for the simple wedge-shaped normal contact, complete closed-form analytical solutions especially for the pressure and tangential tractions have not yet been derived. This is mainly due to the fact that the common solution method involves (strongly) singular integral equations of the second kind, whose explicit solution is challenging. By means of a limiting analysis of the contact with finite friction, Zhupanska & Ulitko (2005) obtained some analytical solutions in form of infinite series for the non-slipping normal contact between a rigid cylinder and an elastic half-plane. Complete solutions were presented by Zhupanska (2012) in a later publication. In the same year Ma & Korsunsky (2012) present an alternative solution based on the Kolosov-Muskhelishvili theory of complex stress functions, which include the case of an elastic-to-elastic contact. Chen & Gao (2006) considered the non-slipping adhesive contact of an elastic cylinder on a stretched substrate and derived a solution in form of integrals which were subsequently evaluated numerically. In a recent paper, Ma & Korsunsky (2022) provide complete solutions in the form of integrals also for the non-slipping normal contact between two elastic bodies whose initial gap is characterized by a monomial function. One of their key results is the frozen-in constant or the so-called interface mismatch eigenstrain, for which they provide integrals including its approximate solutions. As in the work of Ma and Korsunsky, the (strongly) singular integral equations of the second kind are usually taken as the starting point of the solution procedure and subsequently the form of the relative tangential strains within the contact region

is formulated by means of Spence's self-similarity approach. Although a general solution in the form of integrals is available, their evaluation is mathematically so difficult, that, in particular for the pressure distribution and the tangential tractions, closed-form analytical expressions have only been derived for a few exceptions to date. In this paper, we will use this method to derive a few more analytical solutions. However, the focus is on another solution procedure based on the incremental method which allows to derive explicit analytical solutions in a much simpler way. It is capable to determine the interface mismatch eigenstrain as well.

The present work is structured as follows. Section 2 repeats the mathematical formulation of the problem including the singular integral equations of the second kind and the boundary conditions. At the beginning of section 3, the solutions of this singular integral equations are given in terms of integrals to be solved and then applied to determine the analytical solutions for the non-slipping flat-punch contact. Next, based on increments of the flat-punch solution, the new integral equations are deduced, which possess only a weak boundary singularity and are therefore much easier to solve. Section 4 focuses on the derivation of explicit analytical solutions for selected examples, including the symmetric contact with an initial monomial gap profile. The wedge-shaped contact and the contact with an initial parabola gap emerge as special cases from that. Section 5 finally presents explicit analytical solutions for the interface mismatch eigenstrain taking a monomial gap profile function into account.

2. Mathematical Formulation of non-slipping Contact Problems

We begin our considerations with two symmetric, elastic solids that make contact over an (infinite) strip of width 2*a*. Both bodies are regarded as half-spaces, and the contact is caused by a pure normal line loading. Figure 2 shows such a plane strain inducing contact.

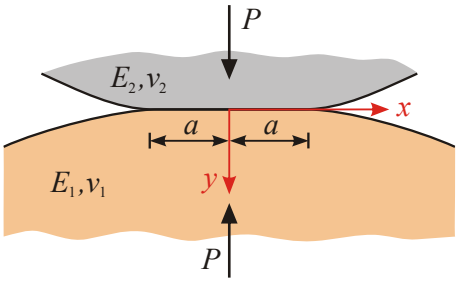

Figure 2. Schematic illustration of a plane contact between two curved, elastic half-spaces under pure normal loading

According to Newton's third law, the distributed pressure $p(x)$ and tangential tractions $q(x)$ act in opposite directions on both bodies within the contact interface resulting in relative surface displacements, denoted by

$$u_x := u_x^{(1)} - u_x^{(2)}, \quad u_y := u_y^{(1)} - u_y^{(2)}. \tag{1}$$

Since the displacements in two-dimensional contact problems are generally logarithmically unbounded relative to the point at infinity, it is common to prefer their derivatives for further analysis. This results in the following coupled integral equations (Johnson, 1985)

$$p(x) + \frac{1}{\pi\beta}\int_{-a}^{a} \frac{q(\xi)\,\mathrm{d}\xi}{x-\xi} = -\frac{E^*}{2\beta} u_x'(x), \tag{2}$$

$$q(x) - \frac{1}{\pi\beta}\int_{-a}^{a} \frac{p(\xi)\,\mathrm{d}\xi}{x-\xi} = +\frac{E^*}{2\beta} u_y'(x), \tag{3}$$

where the effective elastic modulus (composite modulus) and Dundurs' elastic mismatch parameter are defined by

$$E^* := \left(\frac{1-\nu_1^2}{E_1} + \frac{1-\nu_2^2}{E_2}\right)^{-1}, \quad \beta := E^*\left[\frac{(1-2\nu_1)(1+\nu_1)}{2E_1} - \frac{(1-2\nu_2)(1+\nu_2)}{2E_2}\right]. \tag{4}$$

By multiplying Eq. (3) by the imaginary unit and then adding Eq. (2), the two coupled integral equations can be converted into a single complex integral equation

$$F(x)-\frac{i}{\pi\beta}\int_{-a}^{a}\frac{F(\xi)\mathrm{d}\xi}{x-\xi}=-\frac{E^*}{2\beta}\left[u_x'(x)-iu_y'(x)\right], \tag{5}$$

with the complex loading function

$$F(x)=p(x)+iq(x),\quad i=\sqrt{-1}\,. \tag{6}$$

Up to this point, Eqs. (2) and (3) as well as (5) still apply regardless of the prevailing boundary conditions.

For a non-slipping plane normal contact between two bodies with different elastic properties, the following boundary conditions must be satisfied:

$$\frac{\partial}{\partial a}u_x(x,a)=0,\quad u_y'(x)=-f'(x),\quad |q(x)|<\mu p(x),\quad |x|\le a\,. \tag{7}$$

As usual, the second condition relates the slope of the surface to the a priori given derivative of the initial gap function $f(x)$. The third condition aims to ensure full stick in the contact area, i.e., the magnitude of the tangential tractions is insufficient to cause any slip. The first condition, on the other hand, states that the relative tangential displacements within the contact area and thus the relative tangential strains are independent of the contact half-width a. In other words, the relative strain at each point x of the contact area does not change during progressive loading, even though the contact area increases. At first glance this condition makes no prediction about the actual distribution of the relative tangential strains required on the right-hand side of Eq. (5). However, thanks to Spence's self-similarity approach (Spence, 1968) it is possible to infer the shape of the relative tangential strains within the contact area from the shape of the profile. This is explained in more detail below.

3. Methods of Solution

3.1. Singular Integral Equations of the Second Kind

To determine the pressure and tangential tractions within the contact area of the symmetric normal contact, it is necessary to solve Eq. (5). This is a singular integral equation of the second kind, the solution of which was treated in detail by Söhngen (1954):

$$\begin{aligned}F(t)=&\frac{\beta E^*}{2a\left(1-\beta^2\right)}\left[u_x'(t)-iu_y'(t)\right]+\\&+\frac{1}{2\pi\sqrt{1-t^2}}\left(\frac{1+t}{1-t}\right)^{i\eta}\left[\frac{2P}{a\sqrt{1-\beta^2}}+\frac{iE^*}{1-\beta^2}\int_{-1}^{1}\sqrt{1-s^2}\left(\frac{1-s}{1+s}\right)^{i\eta}\frac{u_x'(s)-iu_y'(s)}{a(t-s)}\mathrm{d}s\right],\end{aligned} \tag{8}$$

with the dimensionless variables $t = x/a$ and $s = \xi/a$ as well as the new introduced material mismatch parameter

$$\eta:=\frac{1}{2\pi}\ln\left(\frac{1+\beta}{1-\beta}\right). \tag{9}$$

The solution applies to contacts that exhibit singular pressure and tangential stresses at both edges, such as the indentation of a flat punch with a symmetric cap of any shape under sufficiently high load, so that the cap is in complete contact and the displacements at the contact edges exhibit kinks. However, the solution also holds for contact problems in which singular stresses occur at one edge and bounded ones at the other, or in which bounded pressure and tangential stresses are present at both edges. We restrict ourselves to the latter case, for which the conditions $F(t = \pm 1) = 0$ result in both the calculation equation for the line load P

$$P=-\frac{iE^*}{2\sqrt{1-\beta^2}}\int_{-1}^{1}\frac{s}{\sqrt{1-s^2}}\left(\frac{1-s}{1+s}\right)^{i\eta}\left[u_x'(s)-iu_y'(s)\right]\mathrm{d}s \tag{10}$$

and the consistency condition

$$\int_{-1}^{1} \frac{1}{\sqrt{1-s^2}} \left(\frac{1-s}{1+s}\right)^{i\eta} \left[u_x'(s) - iu_y'(s)\right] \mathrm{d}s = 0 \,. \tag{11}$$

Taking Eqs. (10) and (11) into account, the solution Eq. (8) for the pressure and tangential tractions within the contact area is simplified to

$$F(t) = \frac{\beta E^*}{2a\left(1-\beta^2\right)} \left[u_x'(t) - iu_y'(t)\right] + \frac{iE^*\sqrt{1-t^2}}{2\pi a\left(1-\beta^2\right)} \left(\frac{1+t}{1-t}\right)^{i\eta} \int_{-1}^{1} \left(\frac{1-s}{1+s}\right)^{i\eta} \frac{u_x'(s) - iu_y'(s)}{\sqrt{1-s^2}\,(t-s)} \mathrm{d}s \,. \tag{12}$$

Ma & Korsunsky (2012) present an alternative derivation of the above equations based on the Kolosov-Muskhelishvili theory of complex stress functions and taking into account the displacement boundary conditions.

Once the pressure and tangential tractions within the contact area have been determined, the slope and strain of the surface outside the contact area can in turn be determined from Eqs. (3) and (2). If we consider that no pressure and tangential stresses act on the surface outside the contact area ($|t| > 1$) it follows

$$u_x'(t) - iu_y'(t) = \frac{2ia}{\pi E^*} \int_{-1}^{1} \frac{F(s)}{t-s} \mathrm{d}s \,. \tag{13}$$

3.1.1. Explicit Solutions for Indentation by a Flat Punch

Since the flat punch solution is necessary for the application of the incremental method described below, we first consider this problem which is depicted in Figure 3.

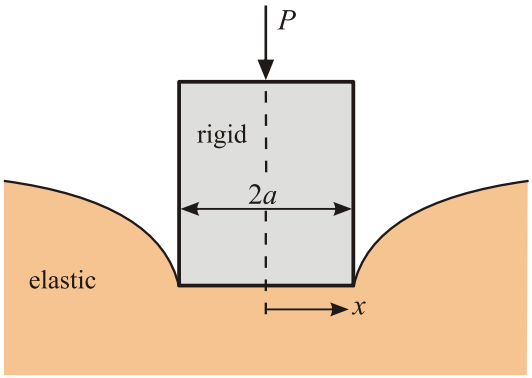

Figure 3. Indentation of an elastic half-plane by a rigid flat punch with the contact half-width *a*

The corresponding displacement boundary conditions are straightforward,

$$u_x'(x) = 0, \quad u_y'(x) = 0, \quad |x| \le a \,. \tag{14}$$

Inserting the boundary conditions (14) into Eq. (8) yields

$$F(t) = \frac{P}{\pi a\sqrt{1-\beta^2}\sqrt{1-t^2}} \left(\frac{1+t}{1-t}\right)^{i\eta}, \tag{15}$$

and, after separating the real and imaginary parts, the distribution of the pressure and tangential stresses within the contact area are found:

$$p(x,P) = \frac{P}{\pi\sqrt{1-\beta^2}\sqrt{a^2-x^2}} \cos\left[\eta \ln\left(\frac{a+x}{a-x}\right)\right], \tag{16}$$

$$q(x,P)=\frac{P}{\pi\sqrt{1-\beta^2}\sqrt{a^2-x^2}}\sin\left[\eta\ln\left(\frac{a+x}{a-x}\right)\right]. \tag{17}$$

Note that the solutions (16) and (17) were first developed by Abramov (1937) using the Mellin transform. To determine the slope and strain of the surface outside the contact area, Eq. (15) has to be inserted into Eq. (13)

$$u_x'(t)-iu_y'(t)=\frac{2iP}{\pi^2E^*\sqrt{1-\beta^2}}\int_{-1}^{1}\frac{1}{(t-s)\sqrt{1-s^2}}\left(\frac{1+s}{1-s}\right)^{i\eta}\mathrm{d}s\,. \tag{18}$$

The calculation of the integral is carried out by Bufler (1959). After appropriate substitution, application of the residual method and separation into real and imaginary parts, the strain and slope of the surface outside the contact area are determined:

$$u_x'(x,P)=-\frac{2P\,\mathrm{sgn}(x)}{\pi E^*\sqrt{x^2-a^2}}\sin\left[\eta\ln\left(\frac{x+a}{x-a}\right)\right], \tag{19}$$

$$u_y'(x,P)=-\frac{2P\,\mathrm{sgn}(x)}{\pi E^*\sqrt{x^2-a^2}}\cos\left[\eta\ln\left(\frac{x+a}{x-a}\right)\right]. \tag{20}$$

3.1.2. The Self-Similarity Approach by Spence for Convex Profiles

The general solutions (8) and (12) of the singular integral equations of the second kind contain integrals whose calculation requires both the slope and the tangential strain in the loaded area. At first glance it seems that apart from a few exceptions such as the indentation by a flat punch, the tangential strains are not known a priori. However, Spence (1968) established a self-similarity approach, which predicts geometrically similar stress and displacement fields during progressive loading for any indenter with a polynomial profile. Even though he initially used this approach only for solving axisymmetric full-stick normal contacts, he already stated its transfer to plane contacts. According to Spence, the distribution of the relative tangential strains within the contact area, also termed interface mismatch eigenstrain, can be deduced from the initial gap function/profile apart from a multiplicative constant. The latter must be determined subsequently from the condition that the stresses at the contact edge vanish. We will apply this often mathematically challenging solution method to an example in Chapter 4.

A much simpler solution method, for which the interface mismatch eigenstrain does not need to be known in advance, is presented in the next section.

3.2. Singular Integral Equations arising from the Incremental Method by Mossakovskii

According to an approach originated by Mossakovskii (1963) for axisymmetric contact problems and revitalized by Jäger (2005), the indentation of an arbitrary convex-shaped body into the elastic half-plane can be described as a sequence of incremental flat punch indentations with different contact half-widths. Therefore, the complete solution of the contact problem (irrespective whether frictionless or under full-stick condition) can be constructed by an appropriate superposition of incremental flat punch solutions with different contact half-widths. Using Eqs. (16) and (17), the incremental contributions of a flat-ended punch of half-width $\tilde{a}$ to pressure and tangential tractions are

$$\mathrm{d}p(x,\tilde{a})=\frac{P'(\tilde{a})\mathrm{d}\tilde{a}}{\pi\sqrt{1-\beta^2}\sqrt{\tilde{a}^2-x^2}}\cos\left[\eta\ln\left(\frac{\tilde{a}+x}{\tilde{a}-x}\right)\right], \tag{21}$$

$$\mathrm{d}q(x,\tilde{a})=\frac{P'(\tilde{a})\mathrm{d}\tilde{a}}{\pi\sqrt{1-\beta^2}\sqrt{\tilde{a}^2-x^2}}\sin\left[\eta\ln\left(\frac{\tilde{a}+x}{\tilde{a}-x}\right)\right]. \tag{22}$$

Obviously, only that flat punch solutions corresponding to half-widths $|x|\le\tilde{a}\le a$ contribute to the stresses at a point x within the contact area. Hence after introducing the dimensionless variables $t = x/a$ and $s = \tilde{a}/a$ and use of the compact complex notation the following formula apply

$$F(t)=\frac{1}{\pi a\sqrt{1-\beta^2}}\int_{|t|}^{1}\frac{P'(s)}{\sqrt{s^2-t^2}}\left(\frac{s+t}{s-t}\right)^{i\eta}\mathrm{d}s\,. \tag{23}$$

Calculation formulae for the displacement derivatives can be deduced in a similar way starting from Eqs. (19) and (20), resulting in

$$u_x'(t)-iu_y'(t)=\frac{2i\,\mathrm{sgn}(t)}{\pi E^*}\int_{0}^{\mathrm{Min}\{|t|,1\}}\frac{P'(s)}{\sqrt{t^2-s^2}}\left(\frac{t+s}{t-s}\right)^{i\eta}\mathrm{d}s\,, \tag{24}$$

where the upper integral limit depends on whether the displacement derivatives are sought inside or outside of the contact area. Compared to the integrals in Eqs. (12) and (13) for calculating the stresses and displacement derivatives, the integrands of the above derived calculation integrals (23) and (24) possess only a weak singularity and are therefore considerably easier to solve, both analytically and numerically. However, their application requires the line load P as a function of the contact half-width. Although this relationship can in principle be determined from Eq. (10), it would not avoid the problem of a priori unknown tangential strains. This is remedied by evaluating the displacement boundary condition in the normal direction (the second condition in Eq. (7)) which relates the slope of the surface to the a priori given derivative of the initial gap function $f(x)$. In this way, by taking the imaginary part of Eq. (24) into account, we obtain

$$\frac{2\,\mathrm{sgn}(t)}{\pi E^*}\int_{0}^{|t|}\frac{P'(s)}{\sqrt{t^2-s^2}}\cos\left[\eta\ln\left(\frac{t+s}{t-s}\right)\right]\mathrm{d}s\overset{!}{=}f'(t)\,. \tag{25}$$

The author is not aware of a general inversion of this integral equation to $P'(s)$. However, if the derivative of the profile function on the right-hand side can be developed into a power series, then $P'(s)$ can also be specified as a power series. As an example, we will prove in the next chapter that a monomial profile function yields a dependence of the line load on the contact half-width, which is characterized by a monomial function of the same order.

Finally, it should be noted that Barber (2018) already lists corresponding general equations, with the difference that he does not use the explicit solutions for the strain and slope of the surface outside the contact area induced by a flat-ended punch according to Eqs. (19) and (20).

4. Derivation of Explicit Solutions for Selected Non-Slipping Contact Problems

To demonstrate the advantages of the incremental method over the solutions of the singular integral equations of second kind in conjunction with Spence's self-similarity approach, the contact problem characterized by a monomial initial gap is first solved in both ways. Subsequently, the wedge-shaped contact and the contact between parabolic cylinders are discussed in detail.

4.1. Symmetric Contact with Initial Monomial Gap Profile

In the following we solve the non-slipping normal contact between two dissimilar elastic bodies whose initial gap is specified by a monomial function according to

$$f(x)=A_n|x|^n,\quad A_n>0,\quad n>0\,. \tag{26}$$

4.1.1. Line load as a Function of the Contact Half-width: Solution by Spence Self-Similarity Approach

By taking the above monomial profile into account the slope of the surface within the contact area becomes

$$u_y'(x)=-nA_n|x|^{n-1}\,\mathrm{sgn}(x),\quad |x|\le a\,, \tag{27}$$

and according to Spence the relative tangential strains within the contact area are distributed by

$$u_x'(x)=nB_n|x|^{n-1},\quad |x|\le a\,. \tag{28}$$

B_n is a constant that is independent of the contact half-width a but a priori unknown. Multiplied by the exponent n it represents the so-called frozen-in strain constant. It is determined by means of the consistency condition (11). This generally leads to

$$B_n = -iA_n \frac{L_{n-1}}{K_{n-1}}, \tag{29}$$

with the definitions

$$K_n := \int_{-1}^{1} \frac{|s|^n}{\sqrt{1-s^2}} \left(\frac{1-s}{1+s}\right)^{i\eta} \mathrm{d}s = 2\int_{0}^{1} \frac{s^n}{\sqrt{1-s^2}} \cos\left[\eta \ln\left(\frac{1-s}{1+s}\right)\right] \mathrm{d}s, \tag{30}$$

$$L_n := \int_{-1}^{1} \frac{|s|^n \operatorname{sgn}(s)}{\sqrt{1-s^2}} \left(\frac{1-s}{1+s}\right)^{i\eta} \mathrm{d}s = 2i\int_{0}^{1} \frac{s^n}{\sqrt{1-s^2}} \sin\left[\eta \ln\left(\frac{1-s}{1+s}\right)\right] \mathrm{d}s. \tag{31}$$

The above governing equations for the frozen-in constant are one of the key results of a recent publication by Ma & Korsunsky (2022). Once the constant has been calculated, the magnitude of the interface mismatch eigenstrain according to Eq. (28) is known as well. However, the determination of this constant is also mandatory for the further calculation of the line load P as a function of the contact half-width a according to Eq. (10) and for the calculation of the contact stresses according to Eq. (12).

By means of partial integration, it is easy to prove that the following recursion formulas apply

$$\{K,L\}_n = \left(1-\frac{1}{n}\right)\{K,L\}_{n-2} - \frac{2\eta i}{n}\{L,K\}_{n-1}, \quad n \geq 2, \tag{32}$$

$$K_1 = 2(1-i\eta L_0), \quad L_1 = -2i\eta K_0. \tag{33}$$

The solutions of the integrals for higher exponents n are therefore determined solely by the solutions of the basic integrals corresponding to $n = 0$. For the determination of the latter, we make use of the substitution $s = \tanh(u/2)$, which then leads to well-known integrals given by Gradshteyn und Ryzhik (2014) in Sect. 3.981 on p. 513:

$$K_0 = \int_{0}^{\infty} \frac{\cos(\eta u)}{\cosh(u/2)} \mathrm{d}u = \frac{\pi}{\cosh(\pi\eta)}, \tag{34}$$

$$L_0 = -i\int_{0}^{\infty} \frac{\sin(\eta u)}{\cosh(u/2)} \mathrm{d}u = i\pi \tanh(\pi\eta) - \psi\left(\frac{1}{4}+i\frac{\eta}{2}\right) + \psi\left(\frac{1}{4}-i\frac{\eta}{2}\right). \tag{35}$$

Herein, $\psi(x)$ denotes the digamma function, also known as the psi-function, which specifies the logarithmic derivative of the gamma function

$$\psi(x) := \frac{\mathrm{d}}{\mathrm{d}x} \ln(\Gamma(x)) = \frac{\Gamma'(x)}{\Gamma(x)}. \tag{36}$$

To determine the line load as a function of the contact half-width, the boundary conditions, Eqs. (27) and (28), are now inserted into Eq. (10) and the relationship (29) subsequently taken into account

$$P(a) = -\frac{iE^* n a^n}{2\sqrt{1-\beta^2}} (L_n B_n + iK_n A_n) = \frac{E^* a^n A_n n}{2\sqrt{1-\beta^2}} \left(\frac{K_n K_{n-1} - L_n L_{n-1}}{K_{n-1}}\right). \tag{37}$$

From the recursion formulas (32) it is easy to deduce

$$n(K_n K_{n-1} - L_n L_{n-1}) = (n-1)(K_{n-1}K_{n-2} - L_{n-1}L_{n-2}) = K_1 K_0 - L_1 L_0 = 2K_0, \tag{38}$$

so that after insertion in Eq. (37) a quite simple expression for the line load as a function of the contact half-width is obtained

$$P(a) = E^* n A_n \kappa(n,\beta) a^n, \quad \kappa(n,\beta) := \frac{\pi}{nK_{n-1}}, \tag{39}$$

where

$$K_{n-1} = \Gamma(n)\Gamma\left(\frac{1}{2}-i\eta\right){}_2\mathrm{F}_1\left(n,\frac{1}{2}-i\eta;\frac{1}{2}+n-i\eta;-1\right)\Big/\Gamma\left(\frac{1}{2}+n-i\eta\right) + \Gamma(n)\Gamma\left(\frac{1}{2}+i\eta\right){}_2\mathrm{F}_1\left(n,\frac{1}{2}+i\eta;\frac{1}{2}+n+i\eta;-1\right)\Big/\Gamma\left(\frac{1}{2}+n+i\eta\right). \tag{40}$$

The factor κ is given for selected exponents of the initial monomial gap function and absolute values of Dundurs' second material mismatch parameter in Table 1. For elastically similar materials ($\beta = 0$), its values correspond to those for frictionless contact (Johnson, 1985).

Table 1. Factor κ for selected absolute values of Dundurs' second material mismatch constant and exponents of the initial monomial gap function

		Exponent *n* of the monomial profile function							
		1	2	3	4	5	6	7	8
$\lvert\beta\rvert$	0	1	0.7854	0.6667	0.5890	0.5333	0.4909	0.4571	0.4295
	0.3	1.0483	0.8429	0.7271	0.6504	0.5949	0.5523	0.5183	0.4903
	0.5	1.1547	0.9789	0.8771	0.8087	0.7590	0.7206	0.6900	0.6648

4.1.2. Line load as a Function of the Contact Half-width: Solution by the Incremental Method

To determine the line load as a function of the contact half-width using the incremental method, we must first derivate the profile function given in Eq. (26) and insert it into Eq (25). This leads to

$$\frac{2}{\pi E^*}\int_0^{|t|}\frac{P'(s)}{\sqrt{t^2-s^2}}\cos\left[\eta\ln\left(\frac{t+s}{t-s}\right)\right]\mathrm{d}s \overset{!}{=} na^n A_n |t|^n . \tag{41}$$

Now we assume that the normal line load we are looking for is a one-term polynomial of the same order n in the contact half-width and that only the polynomial coefficient remains to be determined.

$$P(a) := D_n a^n . \tag{42}$$

After inserting Eq. (42) into Eq. (41) and linear substitution, it follows

$$D_n = \frac{\pi E^* A_n}{2}\Big/\int_0^1\frac{u^{n-1}}{\sqrt{1-u^2}}\cos\left[\eta\ln\left(\frac{1+u}{1-u}\right)\right]\mathrm{d}u = \frac{\pi E^* A_n}{K_{n-1}} . \tag{43}$$

In the last expression on the right-hand side, we have taken the integral definition from Eq. (30) and also considered the point-symmetric argument of the cosine in *u*. After inserting the coefficient into Eq. (42), the function we are looking for is determined.

$$P(a) = \frac{\pi E^* A_n a^n}{K_{n-1}} . \tag{44}$$

The result from Eq. (44) of course agrees with the result from Eq. (39). Note that the integral K_{n-1} was also solved explicitly according to Eq. (40). For the same line load *P*, the contact half-width in the non-slipping normal contact is smaller than that in frictionless contact. This is proven in Figure 4, which shows the ratio of the contact half-widths against the magnitude of Dundurs' second material constant plotted for different monomial power profiles. a_0 denotes the half-width of the corresponding frictionless contact. It is evident that the area reduction is greatest for strongest coupling, i.e., $|\beta| = 0.5$. However, with increasing exponent of the monomial profile function, the area reduction decreases in percentage terms.

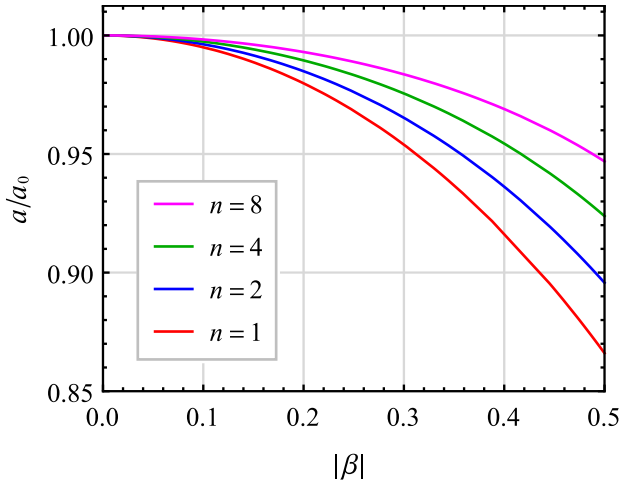

Figure 4. Normalized contact half-width as a function of the magnitude of Dundurs' second material constant plotted for different monomial power profiles

The derivation using the incremental method has proven to be much simpler than that applying the singular integral equations of the second kind in combination with Spence's self-similarity approach. The calculation by the incremental method can be simplified even further since, strictly speaking, it is sufficient to evaluate Eq. (41) at the point $t = 1$ (and thus at the contact edge).

4.1.3. Pressure and Tangential Tractions

To calculate the pressure and tangential tractions within the contact area, we can use either Eq. (12) or Eq. (23). Again, we prefer the formula derived from the incremental method, because the line load has already been determined as a function of the contact half-width and the integral seems easier to solve. From Eq. (44) we easily obtain

$$P'(s) = nP(a)s^{n-1} \tag{45}$$

and after inserting into Eq. (23) the stresses have to be calculated from

$$F(t) = \frac{nP}{\pi a\sqrt{1-\beta^2}} \int_{|t|}^{1} \frac{s^{n-1}}{\sqrt{s^2-t^2}} \left(\frac{s+t}{s-t}\right)^{i\eta} \mathrm{d}s\,. \tag{46}$$

Applying the substitution

$$\varphi(t)u = \frac{s-t}{s+t} \quad \text{with} \quad \varphi(t) := \frac{1-|t|}{1+|t|} \tag{47}$$

provides

$$F(t) = \frac{nP|t|^{n-1}}{\pi a\sqrt{1-\beta^2}} \varphi(t)^{\frac{1}{2}-i\eta\,\mathrm{sgn}(t)} \int_0^1 u^{-\frac{1}{2}-i\eta\,\mathrm{sgn}(t)} \left[1-\varphi(t)u\right]^{-n} \left[1+\varphi(t)u\right]^{n-1} \mathrm{d}u\,. \tag{48}$$

The remaining integral on the right-hand side represents an Appell function $\mathrm{F}_1(\ldots)$, so that the result for the (complex defined) stresses can finally be expressed as follows

$$F(t) = \frac{nP|t|^{n-1}}{\pi a\sqrt{1-\beta^2}} \frac{\mathrm{F}_1\left(\frac{1}{2}-i\eta\,\mathrm{sgn}(t), n, 1-n, \frac{3}{2}-i\eta\,\mathrm{sgn}(t); \frac{1-|t|}{1+|t|}, -\frac{1-|t|}{1+|t|}\right)}{1/2-i\eta\,\mathrm{sgn}(t)} \left(\frac{1-|t|}{1+|t|}\right)^{\frac{1}{2}-i\eta\,\mathrm{sgn}(t)}\,. \tag{49}$$

The Appell function as a generalization of the hypergeometric function to two variables is also defined by the following double series

$$\mathrm{F}_1\left(a,b,b',c;x,y\right) := \sum_{k=0}^{\infty}\sum_{m=0}^{\infty} \frac{\left(a\right)_{k+m}\left(b\right)_k\left(b'\right)_m}{\left(c\right)_{k+m}\,k!m!} x^k y^m,\ \ |x|<1,\ |y|<1,\ \left(z\right)_k := \frac{\Gamma\left(z+k\right)}{\Gamma\left(z\right)}. \tag{50}$$

We leave it at the above compact, complex form (49) and dispense with the explicit formation of real and imaginary parts, which represent the pressure and tangential tractions according to the definition (6). Further simplifications are possible for explicit specifications of n and discussed in more detail below for the wedge-shaped contact ($n = 1$) and the contact between parabolic cylinders ($n = 2$).

Figure 5 illustrates the pressure distribution for selected exponents of the initial monomial gap function. The solid lines represent the case of strongly different elastic materials ($|\beta| = 0.5$) and the dashed lines the corresponding case for elastically similar materials ($\beta = 0$). It can be clearly seen that the pressure in the center is higher due to the coupling. For exponents greater than 2, however, the maximum pressure is no longer in the center. Instead, two maxima are formed symmetrically to the axis of symmetry, which move closer to the edge as the exponent increases. These maxima are weakened by the coupling compared to the frictionless case.

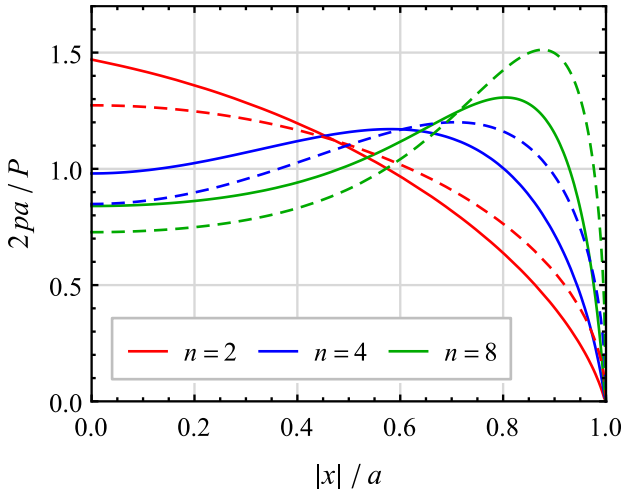

Figure 5. Normalized pressure distribution for selected exponents n of the initial, monomial gap function: Solid lines indicate strong coupling $|\beta| = 0.5$, dashed lines the corresponding frictionless case $\beta = 0$

The tangential stresses (to be continued point-symmetrically) for the case of strong coupling ($|\beta| = 0.5$) illustrated in Figure 6 show that the magnitude of the maxima increases as the exponent grows and also moves towards the contact edge. The magnitude of the tangential stresses is by no means negligible. For larger exponents in particular, the maximum values exceed those of the pressure distribution. There is no need to mention that in the case of elastically similar materials ($\beta = 0$), no tangential stresses occur in the contact interface.

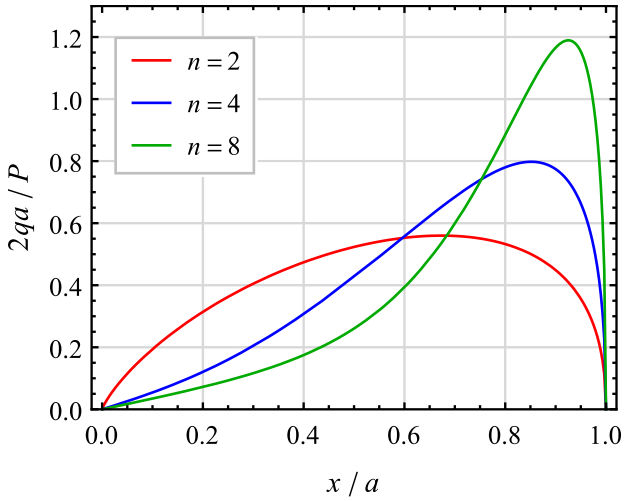

Figure 6. Normalized tangential tractions for selected exponents n of the initial, monomial gap function and strong coupling $|\beta| = 0.5$

4.2. Symmetric Wedge Contact

Now, we consider the non-slipping normal contact with a wedge-shaped initial gap profile. This means that the bodies are brought closer together without load until they touch at exactly one point. The gap between the bodies that then exists is characterized by a linear function. Figure 7 shows an exemplary special case of two bodies under normal loading, where the upper one is assumed to be a very stiff wedge and the lower one a soft half-plane.

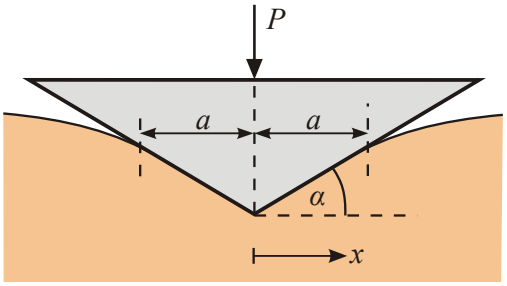

Figure 7. Indentation of an elastic half-plane by a very stiff (rigid) wedge with the slope angle α under full stick condition

In this case, the initial gap is given by the shape of the wedge

$$f(x) = \tan\alpha\,|x| \approx \alpha\,|x|, \tag{51}$$

where small slope angles are required. We can take the line load as a function of the contact half-width directly from Eq. (44) by inserting $n = 1$. This results in

$$P(a) = \frac{\pi E^* A_1 a}{K_0} = \alpha E^* a \cosh(\pi\eta), \tag{52}$$

where we in addition made use of Eq. (34). Taking into account the definition of the material mismatch parameter η according to Eq. (9), we finally get

$$P(a) = \frac{\alpha E^* a}{\sqrt{1-\beta^2}}. \tag{53}$$

To calculate the pressure and tangential stresses, it would also be possible to insert $n = 1$ in the compact form solution (49), but its reduction seems to be more time-consuming than starting again directly from Eq. (23). By taking Eq. (53) into account, the following integral must be solved

$$F(t) = \frac{P}{\pi a\sqrt{1-\beta^2}} \int_{|t|}^{1} \frac{1}{\sqrt{s^2-t^2}} \left(\frac{s+t}{s-t}\right)^{i\eta} \mathrm{d}s \,. \tag{54}$$

After substitution with $u = (s-t)/(s+t)$, an integral representation of the incomplete Beta function denoted by B(...) remains, so that the solution can be written down as follows:

$$F(t) = \frac{P}{\pi a\sqrt{1-\beta^2}} \mathrm{B}\left(\frac{1-|t|}{1+|t|}; \frac{1}{2} - i\eta\,\mathrm{sgn}(t), 0\right). \tag{55}$$

The incomplete Beta function is also defined by

$$\mathrm{B}(z;a,b) := \frac{z^a}{a}\, {}_2\mathrm{F}_1(a, 1-b; 1+a; z) \tag{56}$$

with the hypergeometric function

$${}_2\mathrm{F}_1(a,b;c;z) := \sum_{k=0}^{\infty} \frac{(a)_k (b)_k}{(c)_k} \frac{z^k}{k!}, \quad (x)_k := \frac{\Gamma(x+k)}{\Gamma(x)}. \tag{57}$$

If this series representation is used and the real and imaginary parts are formed, a few algebraic transformations result in the following pressure and tangential tractions:

$$\begin{aligned} p(x,a) = \frac{P}{\pi a\sqrt{1-\beta^2}} \Bigg\{ & \left(\sum_{k=0}^{\infty} \frac{\frac{1}{2}+k}{\left(\frac{1}{2}+k\right)^2+\eta^2} \left(\frac{a-|x|}{a+|x|}\right)^{\frac{1}{2}+k} \right) \cos\left[\eta \ln\left(\frac{a+x}{a-x}\right)\right] \\ & - \mathrm{sgn}(x) \left(\sum_{k=0}^{\infty} \frac{\eta}{\left(\frac{1}{2}+k\right)^2+\eta^2} \left(\frac{a-|x|}{a+|x|}\right)^{\frac{1}{2}+k} \right) \sin\left[\eta \ln\left(\frac{a+x}{a-x}\right)\right] \Bigg\} \end{aligned}, \tag{58}$$

$$\begin{aligned} q(x,a) = \frac{P}{\pi a\sqrt{1-\beta^2}} \Bigg\{ & \left(\sum_{k=0}^{\infty} \frac{\frac{1}{2}+k}{\left(\frac{1}{2}+k\right)^2+\eta^2} \left(\frac{a-|x|}{a+|x|}\right)^{\frac{1}{2}+k} \right) \sin\left[\eta \ln\left(\frac{a+x}{a-x}\right)\right] \\ & + \mathrm{sgn}(x) \left(\sum_{k=0}^{\infty} \frac{\eta}{\left(\frac{1}{2}+k\right)^2+\eta^2} \left(\frac{a-|x|}{a+|x|}\right)^{\frac{1}{2}+k} \right) \cos\left[\eta \ln\left(\frac{a+x}{a-x}\right)\right] \Bigg\} \end{aligned}. \tag{59}$$

For selected material mismatch parameters β, Figure 8 presents the pressure distribution within the contact area, which has a singularity at the tip of the wedge-shaped indenter. The coordinate was normalized with the contact half-width a_0, that would occur in the frictionless state. Apart from a reduced contact half-width, that reached 13.4 percent for $\beta = 0.5$, the curves for different mismatch parameters exhibit no significant differences.

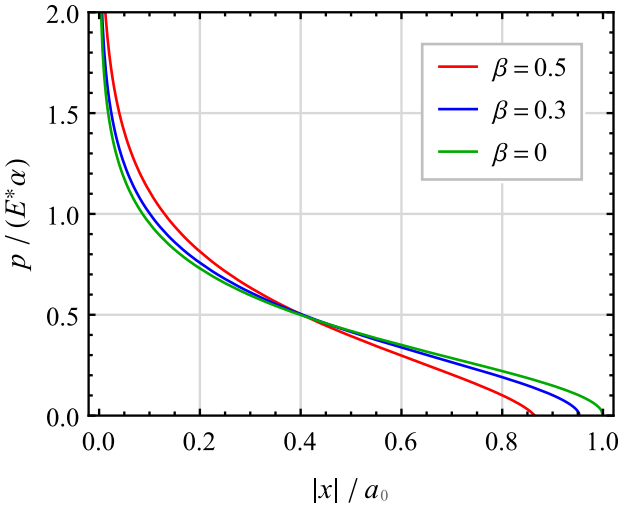

Figure 8. Normalized curves of the pressure when an elastic half-plane is indented by an elastic wedge for selected values of Dundurs' second bimaterial constant

The distribution of the tangential tractions in Figure 9, however, reveals a characteristic feature. Considering that they are distributed point-symmetrically to the origin, a jump can be observed at the point $x = 0$, which is due to the non-differentiability of the profile at this point.

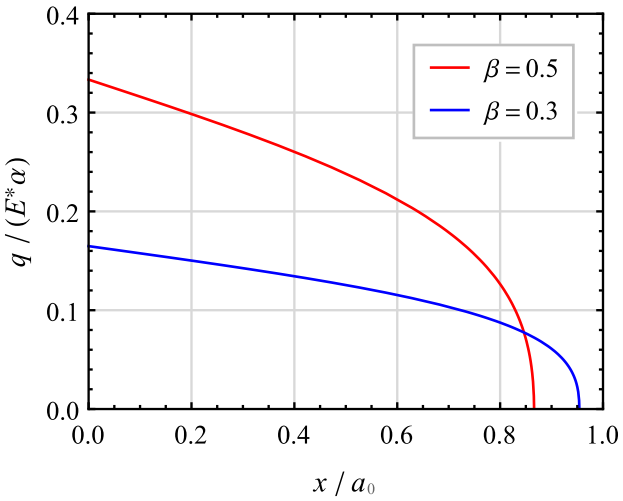

Figure 9. Normalized curves of the tangential tractions within the contact area of the non-slipping normal contact between an elastic wedge and an elastic half-plane for selected values of Dundurs' second bimaterial constant

4.3. Symmetric Parabola Contact

In the following, we consider the classic case of an initial gap in the form of a parabola, which both Zhupanska (2012) and Ma & Korsunsky (2012) treated in different ways but using Spence's self-similarity approach. Figure 10 schematically displays the limiting case of a rigid parabolic cylinder with the radius of curvature R, which is pressed into an elastic half-plane under full-stick assumption.

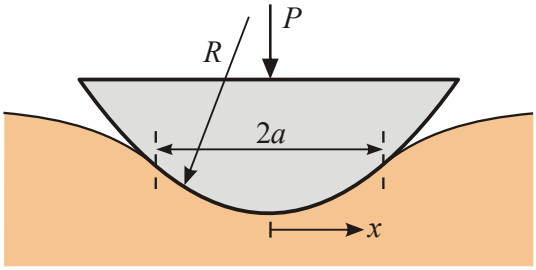

Figure 10. Indentation of an elastic half-plane by a very stiff (rigid) parabolic cylinder with radius of curvature *R* under full stick condition

The profile function is given by

$$f(x)=\frac{x^2}{2R},\quad |x|\le a\,. \tag{60}$$

Now, we again prefer to apply the equations that have emerged from the incremental method. For this purpose, the line load is required as a function of the half-contact width, which results from Eq. (44) if $n = 2$ is inserted

$$P(a)=\frac{\pi E^* A_2 a^2}{K_1}\,. \tag{61}$$

Taking Eqs. (33) and (35) into account, then it follows

$$P(a)=\frac{\pi E^* a^2}{4R}\left\{1+\pi\eta\tanh(\pi\eta)+i\eta\left[\psi\left(\frac{1}{4}+i\frac{\eta}{2}\right)-\psi\left(\frac{1}{4}-i\frac{\eta}{2}\right)\right]\right\}^{-1}\,. \tag{62}$$

Now, since the line load is known as a function of the contact half-width, Eq. (23) can be used to calculate the pressure and tangential tractions. A reduction of the double sum of the Appell function in Eq. (49) is also possible, but appears to be more elaborate. By means of Eq. (62) and using partial integration, we obtain

$$F(t)=\frac{2P}{\pi a\sqrt{1-\beta^2}}\left[\sqrt{1-t^2}\left(\frac{1+t}{1-t}\right)^{i\eta}+2i\eta t\int_{|t|}^{1}\frac{1}{\sqrt{s^2-t^2}}\left(\frac{s+t}{s-t}\right)^{i\eta}\mathrm{d}s\right]. \tag{63}$$

A solution of the remaining integral on the right-hand side has already been given when dealing with the wedge-shaped contact from the last section (see Eqs. (54) to (55))

$$F(t)=\frac{2P}{\pi a\sqrt{1-\beta^2}}\left\{\sqrt{1-t^2}\left(\frac{1+t}{1-t}\right)^{i\eta}+2i\eta t\mathrm{B}\left(\frac{1-|t|}{1+|t|};\frac{1}{2}-i\eta\,\mathrm{sgn}(t),0\right)\right\}. \tag{64}$$

After taking the real and imaginary part as well as using the series representation according to Eqs. (56) and (57) a few algebraic transformations yield the following solutions

$$p(x,a)=\frac{2P}{\pi a^2\sqrt{1-\beta^2}}\left\{\left(\sqrt{a^2-x^2}-2\eta^2|x|\sum_{k=0}^{\infty}\frac{1}{\left(\frac{1}{2}+k\right)^2+\eta^2}\left(\frac{a-|x|}{a+|x|}\right)^{\frac{1}{2}+k}\right)\cos\left[\eta\ln\left(\frac{a+x}{a-x}\right)\right]\right.$$
$$\left.-2\eta x\left(\sum_{k=0}^{\infty}\frac{\frac{1}{2}+k}{\left(\frac{1}{2}+k\right)^2+\eta^2}\left(\frac{a-|x|}{a+|x|}\right)^{\frac{1}{2}+k}\right)\sin\left[\eta\ln\left(\frac{a+x}{a-x}\right)\right]\right\}, \tag{65}$$

$$q(x,a)=\frac{2P}{\pi a^2\sqrt{1-\beta^2}}\left\{\left(\sqrt{a^2-x^2}-2\eta^2|x|\sum_{k=0}^{\infty}\frac{1}{\left(\frac{1}{2}+k\right)^2+\eta^2}\left(\frac{a-|x|}{a+|x|}\right)^{\frac{1}{2}+k}\right)\sin\left[\eta\ln\left(\frac{a+x}{a-x}\right)\right]\right. \quad (66)$$
$$\left.+2\eta x\left(\sum_{k=0}^{\infty}\frac{\frac{1}{2}+k}{\left(\frac{1}{2}+k\right)^2+\eta^2}\left(\frac{a-|x|}{a+|x|}\right)^{\frac{1}{2}+k}\right)\cos\left[\eta\ln\left(\frac{a+x}{a-x}\right)\right]\right\}.$$

Note that similar power series representations leading to equal values were determined by Zhupanska (2012) by a different method. Figure 11 shows the distribution of pressure within the contact area for selected material mismatch parameters β under the same applied line load P. It should be noted that the coordinate was normalized with the contact half-width a_0, which would occur in the decoupled state (plane Hertzian contact). Similarly, the pressure distribution was related to the mean pressure of the uncoupled contact. While the normalized pressure maximum for strongly dissimilar materials (β = 0.5) is significantly greater than in the contact between bodies made of elastically similar materials (β = 0), the difference for realistic values β ≈ 0.2-0.3 is much smaller. Therefore, the pressure distribution in this range is often approximated by that of the frictionless contact, which is tantamount to neglecting the influence of the tangential stresses on the normal displacement.

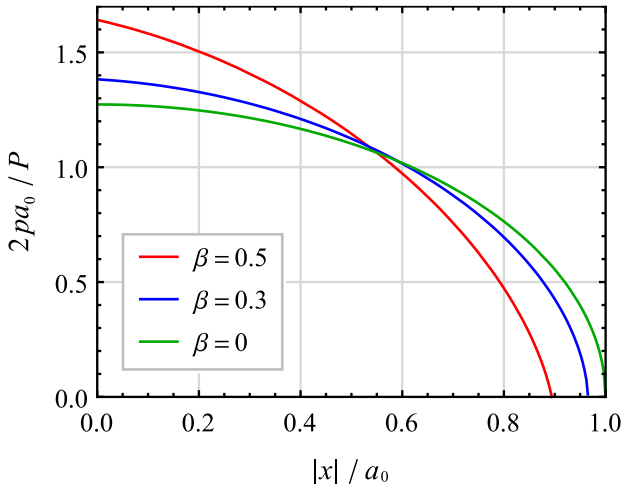

Figure 11. Normalized curves of the pressure when an elastic half-plane is indented by an elastic parabolic cylinder for selected values of Dundurs' second bimaterial constant

However, the fact that the pressure contributes significantly to the tangential displacement and thus influence the distribution of the tangential tractions is supported by Figure 12.

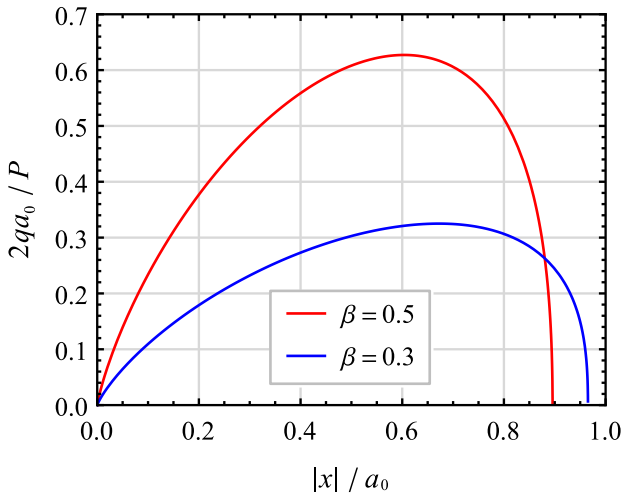

Figure 12. Normalized tangential tractions within the non-slipping normal contact of an elastic parabolic cylinder and an elastic half-plane distinguished according to values of Dundurs' second bimaterial constant

5. The Interface Mismatch Eigenstrain

Before material points of the two half-space surfaces come into contact during progressive loading, they undergo different tangential displacements because of material property mismatch. As soon as they make contact under full-stick condition, their relative tangential displacement and thus their relative tangential strain were frozen-in, i.e., they do not change when the size of the contact area increases due to further loading. The corresponding strain is termed frozen-in strain or interface mismatch eigenstrain. By exploiting Spence's self-similarity approach, that assumes their distribution to be consistent with the gap profile, we have already determined these strains for an initial monomial gap profile (see Eqs. (27) to (31)). But even without using self-similarity, their calculation is possible in a straightforward manner. For this purpose, we apply Eq. (24) within the contact area

$$u_x'(t) = -\frac{2\,\mathrm{sgn}(t)}{\pi E^*}\int_0^{|t|}\frac{P'(s)}{\sqrt{t^2-s^2}}\sin\left[\eta\ln\left(\frac{t+s}{t-s}\right)\right]\mathrm{d}s, \quad |t|<1. \tag{67}$$

Let us again suppose that the initial gap profile is specified by a monomial function according to Eq. (26) and the line load has already been determined as a function of the contact half-width. Then, after substituting Eq. (45) into Eq. (67) and taking Eq. (44) into account, it is easy to prove that holds

$$u_x'(t) = \frac{2nA_n a^n |t|^{n-1}}{K_{n-1}}\int_0^1\frac{z^{n-1}}{\sqrt{1-z^2}}\sin\left[\eta\ln\left(\frac{1-z}{1+z}\right)\right]\mathrm{d}z\,. \tag{68}$$

The integral on the right-hand side is part of the definition (31) and can for example be solved with recursion formulas (32) to (35). With this definition, the mismatch eigenstrain can finally be notated as follows

$$u_x'(x) = -inA_n|x|^{n-1}\frac{L_{n-1}}{K_{n-1}}\,. \tag{69}$$

Hence, the results (28) and (29) stemming from the self-similarity approach are verified. Relating the eigenstrain to the magnitude of the derivative of the profile function, yields the normalized frozen-in constant

$$\gamma_n := \frac{u_x'(x)}{f'(x)\,\mathrm{sgn}(x)} \equiv \frac{B_n}{A_n} = \frac{-iL_{n-1}}{K_{n-1}}\,. \tag{70}$$

Taking Eqs. (34) and (35) into account, for an initial wedge-shaped profile gap Eq. (70) provides

$$\gamma_1 = \frac{-iL_0}{K_0} = \sinh(\pi\eta) + \frac{\cosh(\pi\eta)}{\pi}\left[i\psi\left(\frac{1}{4}+i\frac{\eta}{2}\right) - i\psi\left(\frac{1}{4}-i\frac{\eta}{2}\right)\right]. \tag{71}$$

As a further example a parabolic profile gap leads to

$$\gamma_2 = \frac{-iL_1}{K_1} = \frac{-\eta K_0}{1-i\eta L_0} = \frac{-\pi\eta}{\pi\eta\sinh(\pi\eta) + \cosh(\pi\eta)\left[1+i\eta\psi\left(\frac{1}{4}+i\frac{\eta}{2}\right) - i\eta\psi\left(\frac{1}{4}-i\frac{\eta}{2}\right)\right]}. \tag{72}$$

If the difference of the digamma functions is replaced by infinite series, then alternatively holds

$$\gamma_2 = \frac{-\pi\eta}{\cosh(\pi\eta)\left(1+\pi\eta\tanh(\pi\eta) - 16\eta^2\sum_{k=0}^{\infty}\frac{1}{(1+4k)^2+4\eta^2}\right)}. \tag{73}$$

It should be mentioned that the frozen-in constants derived by Zhupanska (2012) and Ma & Korsunsky (2012) contain alternating series and thus seems to deviate from Eq. (73) at first glance. However, all formulations provide identical values for any material mismatch. For the two profiles focused above and other selected monomial profile functions, Figure 13 demonstrates the dependence of the normalized frozen-in constant on Dundurs' second bimaterial constant. The curves must be continued point-symmetrically to the origin. Ma & Korsunsky (2012) already pointed out that (the magnitude of) the normalized frozen-in constant (they termed it correlation coefficient) is gradually increasing with the order of the monomial function.

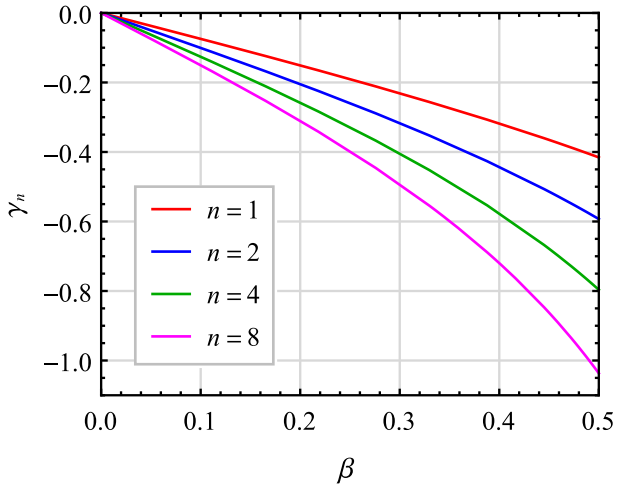

Figure 13. Normalized frozen-in constant as a function of Dundurs' second material mismatch parameter for selected exponents of the monomial gap function

6. Conclusions

In this work, we have deduced singular integral equations by means of the incremental method, which allow to solve plane non-slipping normal contacts in a much simpler way than the commonly used singular integral equations. On the one hand, this is due to the fact that the integrands only exhibit a weak boundary singularity and, on the other hand, that Spence's self-similarity approach and thus the prior calculation of the relative tangential strain are not required. However, the normal force as a function of the contact half-width must have been determined in advance. In this way, we were able to derive some new closed-form solutions, especially for the non-slipping normal contact between elastically dissimilar bodies whose initial gap profile is specified by a monomial function. Since the interface mismatch eigenstrain is also of interest for many practical contact problems, integral equations were also established for its calculation based on the incremental method. For the above-mentioned contact configuration, closed-form analytical solutions for these relative tangential strains were derived. For complex coupled problems, the Goodman approximation is often used to obtain an analytical approximate solution. Corresponding integral equations can also be developed using the incremental method. A major advantage of the Goodman approximation is that the

pressure distribution is taken from the frictionless contact and thus the normal force as a function of the contact half-width is a priori known. As an example, the simply derivable formula for calculating the tangential tractions is listed below

$$q(x)=\frac{\beta}{\pi^2}\int_{|x|}^{a}\frac{P'(\tilde{a})}{\sqrt{\tilde{a}^2-x^2}}\ln\left(\frac{\tilde{a}+x}{\tilde{a}-x}\right)\mathrm{d}\tilde{a}\ . \tag{74}$$

In the present work, the incremental method was used to derive integral equations applicable for solving plane normal contacts under full stick condition. However, analogous equations can also be derived in the same way under the more realistic condition of partial slip. This is possible due to an inherent feature of all normal contact problems characterized by a convex initial gap function under partial slip, which goes back to a finding by Spence (1973). Accordingly, although both the stick area and the (total) contact area increase during progressive loading their ratio remains constant and is equal to the ratio obtained from the corresponding flat-ended punch problem.

Acknowledgement: The author is grateful to Dr. Lifeng Ma for the professional discussions on normal contact problems under full stick condition.

References

Abramov, B. M. (1937). The problem of contact of an elastic infinite half-plane with an absolutely rigid rough foundation. Comptes Rendus de l'Académie des Sciences de l'URSS, 17, 173–178.

Barber, J. R. (2018). Contact mechanics. Springer, (Chapter 7). https://doi.org/10.1007/978-3-319-70939-0_7

Borodich, F. M., Galanov, B. A., & Suarez-Alvarez, M. M. (2014). The JKR-type adhesive contact problems for power-law shaped axisymmetric punches. Journal of the Mechanics and Physics of Solids, 68, 14–32. https://doi.org/10.1016/j.jmps.2014.03.003

Bufler, H. (1959). Einige strenge Lösungen für den Spannungszustand in ebenen Verbundkörpern. ZAMM Zeitschrift für Angewandte Mathematik und Mechanik, 39(5-6), 218–236. https://doi.org/10.1002/zamm.19590390507

Chen, S., & Gao, H. (2006). Non-slipping adhesive contact of an elastic cylinder on stretched substrates. Proceedings of the Royal Society A: Mathematical, Physical and Engineering Sciences, 462(2065), 211–228. https://doi.org/10.1098/rspa.2005.1553

Chen, S., & Gao, H. (2007). Bio-inspired mechanics of reversible adhesion: orientation-dependent adhesion strength for non-slipping adhesive contact with transversely isotropic elastic materials. Journal of the Mechanics and Physics of Solids, 55(5), 1001–1015. https://doi.org/10.1016/j.jmps.2006.10.008

de Payrebrune, K. M. (2022). Relation of kinematics and contact forces in three-body systems with a limited number of particles. Facta Universitatis, Series: Mechanical Engineering, 20(1), 095–108. https://doi.org/10.22190/FUME210310035P

Guo, X., Jin, F., & Gao, H. (2011). Mechanics of non-slipping adhesive contact on a power-law graded elastic half-space. International Journal of Solids and Structures, 48(18), 2565–2575. https://doi.org/10.1016/j.ijsolstr.2011.05.008

Gradshteyn, I. S., & Ryzhik, I. M. (2014). Table of integrals, series, and products. (8th ed.). Academic press. https://doi.org/10.1016/C2010-0-64839-5

Heß, M. (2011). Über die exakte Abbildung ausgewählter dreidimensionaler Kontakte auf Systeme mit niedrigerer räumlicher Dimension. Cuvillier Verlag. Göttingen.

Jäger, J. (2005). New Solutions in Contact Mechanics. WIT Press. Southampton, Boston.

Johnson, K. L. (1985). Contact Mechanics. Cambridge University Press. Cambridge.

Li, Q. (2020). Simulation of a single third-body particle in frictional contact. Facta Universitatis, Series: Mechanical Engineering, 18(4), 537–544. https://doi.org/10.22190/FUME201002045L

Luo, Q. H., & Zhou, Y. T. (2022). Adhesive contact behavior between piezoelectric and elastic materials with a mismatch strain. Acta Mechanica, 233(2), 617–639. https://doi.org/10.1007/s00707-021-03120-3

Ma, L., & Korsunsky, A. M. (2012). Complex variable formulation for non-slipping plane strain contact of two elastic solids in the presence of interface mismatch eigenstrain. International Journal of Solids and Structures, 49(9), 1177–1188. https://doi.org/10.1016/j.ijsolstr.2012.02.002

Ma, L., & Korsunsky, A. M. (2022). Interface mismatch eigenstrain of non-slipping contacts between dissimilar elastic solids. International Journal of Solids and Structures, 253, 111760. https://doi.org/10.1016/j.ijsolstr.2022.111760

Mossakovskii, V. I. (1963). Compression of elastic bodies under conditions of adhesion (axisymmetric case). Journal of Applied Mathematics and Mechanics, 27(3), 630–643. https://doi.org/10.1016/0021-8928(63)90150-3

Nowell, D., Hills, D. A., Sackfield, A. (1988). Contact of dissimilar elastic cylinders under normal and tangential loading. Journal of the Mechanics and Physics of Solids, 36(1), 59–75. https://doi.org/10.1016/0022-5096(88)90020-8

Popov, G. I. (1973). Axisymmetric contact problem for an elastic inhomogeneous half-space in the presence of cohesion. Journal of Applied Mathematics and Mechanics, 37(6), 1052–1059. https://doi.org/10.1016/0021-8928(73)90070-1

Popov, V. L., & Heß, M. (2015). Method of dimensionality reduction in contact mechanics and friction. Springer Berlin Heidelberg. https://doi.org/10.1007/978-3-642-53876-6

Popov, V. L., Heß, M., & Willert, E. (2019). Handbook of contact mechanics: exact solutions of axisymmetric contact problems. Springer Nature. https://doi.org/10.1007/978-3-662-58709-6

Söhngen, H. (1954). Zur Theorie der endlichen Hilbert-Transformation. Mathematische Zeitschrift, 60, 31–51. https://doi.org/10.1007/BF01187356

Spence, D. A. (1968). Self similar solutions to adhesive contact problems with incremental loading. Proceedings of the Royal Society of London, Series A, Mathematical and Physical Sciences, 305(1480), 55–80. https://doi.org/10.1098/rspa.1968.0105

Spence, D. A. (1973). An eigenvalue problem for elastic contact with finite friction. In Mathematical Proceedings of the Cambridge Philosophical Society, 73(1), 249–268. https://doi.org/10.1017/S0305004100047666

Zhupanska, O. I., & Ulitko, A. F. (2005). Contact with friction of a rigid cylinder with an elastic half-space. Journal of the Mechanics and Physics of Solids, 53(5), 975–999. https://doi.org/10.1016/j.jmps.2005.01.002

Zhupanska, O. I. (2009). Axisymmetric contact with friction of a rigid sphere with an elastic half-space. Proceedings of the Royal Society A: Mathematical, Physical and Engineering Sciences, 465(2108), 2565–2588. https://doi.org/10.1098/rspa.2009.0109

Zhupanska, O. I. (2012). Adhesive full stick contact of a rigid cylinder with an elastic half-space. International Journal of Engineering Science, 55, 54–65. https://doi.org/10.1016/j.ijengsci.2012.02.002